ChemPubSoc Europe

DOI: 10.1002/chem.201304714

CHEMISTRY A European Journal Full Paper

Self-Assembly

Out-of-Water Constitutional Self-Organization of Chitosan–Cinnamaldehyde Dynagels

Luminita Marin,[a] Simona Moraru,[a] Maria-Cristina Popescu,[a] Alina Nicolescu,[a] Cristina Zgardan,[a] Bogdan C. Simionescu,[a, b] and Mihail Barboiu*[a, c]

Abstract: An investigation of the constitutional adaptive gelation process of chitosan/cinnamaldehyde (**C**/**Cy**) dynagels is reported. These gels generate timely variant macroscopic organization across extended scales. In the first stage, imine-bond formation takes place "in-water" and generates low-ordered hydrogels. The progressive formation of imine bonds further induces "out-of-water" increased reactivity within interdigitated hydrophobic self-assembled layers of **Cy**, with a protecting environmental effect against hydrolysis and that leads to the stabilization of the imine bonds. The hydrophobic swelling due to **Cy** layers at the interfaces reaches a critical step when lamellar self-organized hybrids are generated (24 hours). This induces an important restructuration of the hydrogels on the micrometric scale, thus resulting in the formation of highly ordered microporous xerogel morphologies of high potential interest for chemical separations, drug delivery, and sensors.

Introduction

Constitutional dynamic chemistry (CDC) brings into play the self-evolution of dynamic molecular and supramolecular systems toward the selection of discrete architectures from mixtures of exchanging components.[1] The self-assembling of the components into adaptive architectures across size scale, controlled by mastering constitutional affinities, embodies the flow of structural information from the molecular level toward nanoscale/microscale dimensions.[2]

Within this context, we recently proved that the progressive incorporation of hydrophobic synthons through imine-bond formation onto hydrophilic chitosan backbones produces the depletion of strongly hydrogen-bonded chitosan chains, thus resulting, in some cases, in the formation of stable chitosan hydrogels, films, or powders, which are a function of the nature of the grafted moiety in the Chitosan backbones.[3] The reorganization of hydrophobic/hydrophilic systems is probably connected to 1) a protecting environmental effect against hydrolysis and the stabilization of the reversible imino bonds at the molecular level[3a] and 2) the self-control of the balance of interactions, which is a determinant for the emergence of novel solid-phase formation and materials at the supramolecular level.[3b]

Previous studies in our laboratories[3a] have shown that among different formulations (i.e., films or powders)[3b] that can be obtained from various aldehydes, stable hydrogels can be prepared by treating cinnamaldehyde (**Cy**) with chitosan (**C**; Scheme 1).[3] Although the control of the hydrogel formation seems to be reasonable, the dynamic reversible equilibrium of the **Cy** imine-bond formation at the molecular level cumulated and the self-organization of **C**/**Cy** hydrophilic/hydrophobic supramolecular interfaces remain key challenges.

More generally, the formation of "dynamic gels" (i.e., dynagels) dynamic on both the molecular and supramolecular levels is reminiscent of a number of other nonexclusive constitutional systems, including helical and lamellar nanometric hybrid phases,[4a–c] cholesteric lyotropic systems,[4d] constitutional dynamic gels,[4e,f] self-replicating dynablocks[4g] or dynasurfaces,[4h] and so forth.

Herein, we report the investigation of the dynamic constitutional gelation process of **C**/**Cy** hydrogels and of the characteristics of the corresponding xerogels in an attempt to extend and engineer constitutional interactions to generate timely variant-adaptive macroscopic organization of **C**/**Cy** dynagels across extended scales.[2]

C/**Cy** hydrogels have been obtained by mixing solutions of **C** and **Cy** in water and acetone, respectively, at various $\mathbf{C}_{NH2}$/$\mathbf{Cy}_{CHO}$ molar ratios at 50 °C (see Scheme 1 and Table 1).

[a] *Dr. L. Marin, Dr. S. Moraru, Dr. M.-C. Popescu, A. Nicolescu, C. Zgardan, Prof. Dr. B. C. Simionescu, Dr. M. Barboiu*
"Petru Poni" Institute of Macromolecular Chemistry of Romanian Academy, 41A Aleea Gr. Ghica Voda, Iasi (Romania)

[b] *Prof. Dr. B. C. Simionescu*
"Gheorghe Asachi" Technical University of Iasi
73 Strada Prof. Dimitrie Mangeron, Iasi (Romania)

[c] *Dr. M. Barboiu*
Institut Européen des Membranes, ENSCM-UMII-CNRS 5635
IEM/UM2, CC 047, Place Eugène Bataillon
34095, Montpellier, Cedex 5 (France)
E-mail: mihail-dumitru.barboiu@univ-montp2.fr

Supporting information for this article is available on the WWW under http://dx.doi.org/10.1002/chem.201304714.

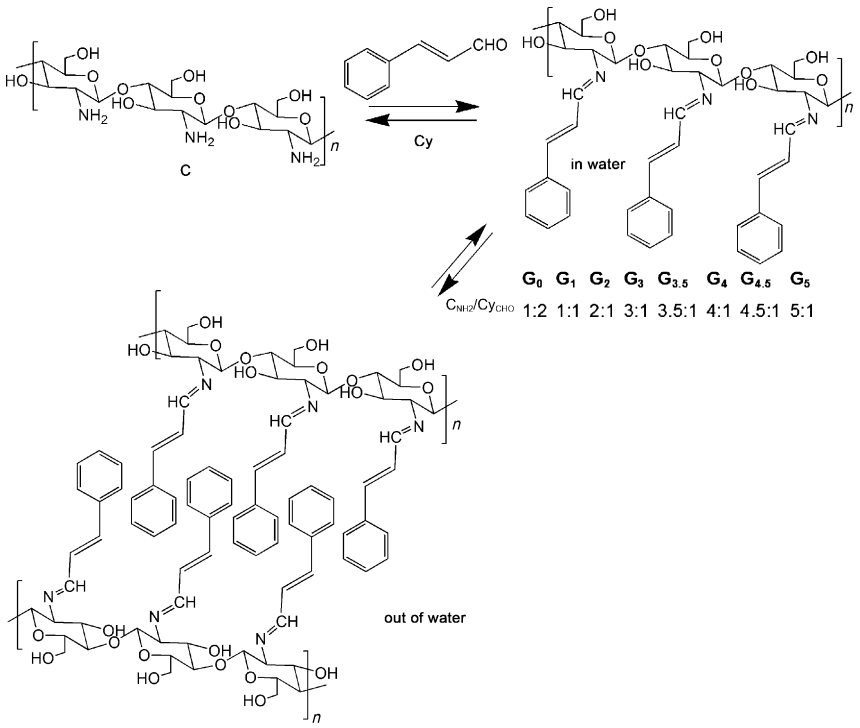

Scheme 1. Synthesis of G_0–G_5 hydrogels through the reversible molecular imino-bonding of **Cy** and hydrophilic/hydrophobic supramolecular self-organization, thus giving rise to "in-water" and "out-of-water" populations of the hydrophobic **Cy** component (see Table 1 for the composition of the G_0–G_5 hydrogels).

Table 1. The molar ratio of functional units and corresponding hydrogel codes.[a]

Code	G_0	G_1	G_2	G_3	$G_{3.5}$	G_4	$G_{4.5}$	G_5
C_{NH2}/Cy_{CHO}	1:2	1:1	2:1	3:1	3.5:1	4:1	4.5:1	5:1

[a] Calculated as the molar ratio of glucosamine repeat units to cinnamaldehyde.

Results and Discussion

Chitosan and cinnamaldehyde as important molecules in bioapplications

Chitosan, a natural biopolymer obtained by the deacetylation of chitin, has proved to possess many outstanding biological properties, namely, biocompatibility, nontoxicity (its degradation products are known natural metabolites), non-antigenicity, antitumoral activity, and haemostatic, antimicrobial, fungistatic, spermicidal, central-nervous-system-depressant, and immune-adjuvant properties. The abilities of this compound to improve wound healing or blood clotting; form protective films and coatings; selectively bind acidic liquids, thereby lowering serum cholesterol levels (hypertension prevention); and accelerate bone formation or environmental protection results in the utilization of chitosan in a huge "workbench" for researchers in various domains, especially those addressing bioapplications.[5–7] One important use of chitosan is related to its hydrogels due to their presence in a large number of biomedical, cosmetics, personal-care, food, and environment-protection applications, and so forth. Chitosan hydrogels can be prepared without any crosslinking agent,[9] but are usually obtained through the formation of bridges between chitosan backbones. The hydrogen-bonding interactions can be modified by imine covalent linkages when the free amino groups on chitosan react with monoaldehydes or appropriate difunctional cross-linkers, such as glutaraldehyde,[10] terephthaldehyde,[11] diisocyanate,[12] and formaldehyde,[13] when chemical hydrogels are obtained. Relative to physical hydrogels, the chemical hydrogels are permanent and quite robust networks owing to the presence of covalent cross-linking agents. Recent studies have demonstrated that usual cross-linkers, such as glutaraldehyde, are in fact toxic,[14,15] and the attention of researchers has focused on other cross-linkers to yield more environmentally and health-friendly hydrogels appropriate for bioapplications.

Cinnamaldehyde is a natural extracted oil used as a flavoring agent and has proved to have a lot of beneficial properties, such as hypoglycemic and hypolipidic characteristics, and thus is a potential antidiabetic agent[16] with a shown vasodilator effect,[17] antipathogenic[18] activity against both gram-positive and -negative bacteria,[19] antimicrobial[20] or antifungal activities,[21] and inhibition of the proliferation of several human cancer-cell lines including breast, ovarian, lung, and colon carcinomas and leukaemia.[22] Besides, in vivo studies established that the acceptable daily intake can reach 73.5 mg kg^{-1} body weight day^{-1}.[22]

Systems containing both chitosan and cinnamaldehyde should present interesting synergetic effects. The antimicrobial properties of Schiff bases from chitosan and cinnamaldehyde formed under high-intensity ultrasound have been recently reported.[23] The delivery of baicalein by using cinnamaldehyde/chitosan systems has been explored too, but no information on the composite hydrogels was provided.[23] The reversible covalent nature of the imine linkage (C=N) allows the aldehyde subcomponents to be independently displaced in well-defined ways, thus allowing the formation of nanostructured architectures.[25]

Hydrogel synthesis

A 3% solution of cinnamaldehyde in acetone was added slowly to a 2% solution of chitosan (0.05 g, 0.29 mmol glucos-

amine repeat units) in 0.7% acetic acid (optimal amount for the **C** solubilization)[9] with vigorous stirring at 50 °C. The amount of **Cy** was varied to give molar ratios of $\mathbf{C}_{NH2}/\mathbf{Cy}_{CHO}$ (Table 1). The hydrogel formation was practically achieved in few minutes, except for mixtures of 4:1 and 4.5:1 $\mathbf{C}_{NH2}/\mathbf{Cy}_{CHO}$, when the hydrogels were formed by cooling at room temperature, although the 5:1 mixture remained a viscous liquid.

The hydrogels were lyophilized to give the corresponding xerogels to follow their morphology. The gels were flash frozen in liquid nitrogen and lyophilized for 24 hours with a Martin Christ Alpha 1-2LD freeze-dryer system.

HRMAS spectroscopic analysis

The reaction between **C** and **Cy** was quantified through High-resolution magic-angle spinning (HRMAS) and 2D NMR experiments performed in $D_2O/(CD_3)_2CO$ (Figure 1). The spectra allowed easy identification of the peaks that correspond to the partial conversion of chitosan **C** into $\mathbf{G_0}$–$\mathbf{G_5}$ hydrogels: $\delta = 3$–5 ppm for the C backbone protons;[26] $\delta = 6$–8 ppm for aromatic **Cy** protons; interestingly, pairs of signals, a doublet and a broad singlet at $\delta = 8.20$ and 8.44 ppm, respectively, that belong to the -C*H*=N- group; and a doublet and a broad singlet at $\delta = 9.50$ and 9.10 ppm, respectively, that belong to the starting-material -C*H*=O group (Figure 1a). These signals were assigned by using ^{1}H NMR spectroscopy: the spectrum of **Cy** was recorded in D-acetone and shows the solvated **Cy** aldehyde proton at $\delta = 9.50$ ppm, whereas the spectrum registered in D_2O shows the appearance of a supplementary "out-of-water" **Cy** aldehyde proton peak at $\delta = 9.03$ ppm (Figure 1b,c). By analogy, the resulting chitosan imine bonds can be considered to present similar behavior, that is, a sharp peak and a broad peak at $\delta = 8.5$ and 8.1 ppm for the "in-water" and "out-of-water" imine groups, respectively. The "out-of-water" formation of the imine groups might be stabilized at the hydrophobic interfaces, which resulted through the self-assembly of **Cy** components along the chitosan backbones (see below), with a protective environmental effect against hydrolysis (Scheme 1). As expected, the yield of the imine formation increases with increasing excess of the **C** amino groups; consequently, the reaction is almost quantitative for $\mathbf{G_4}$ (Table 2).

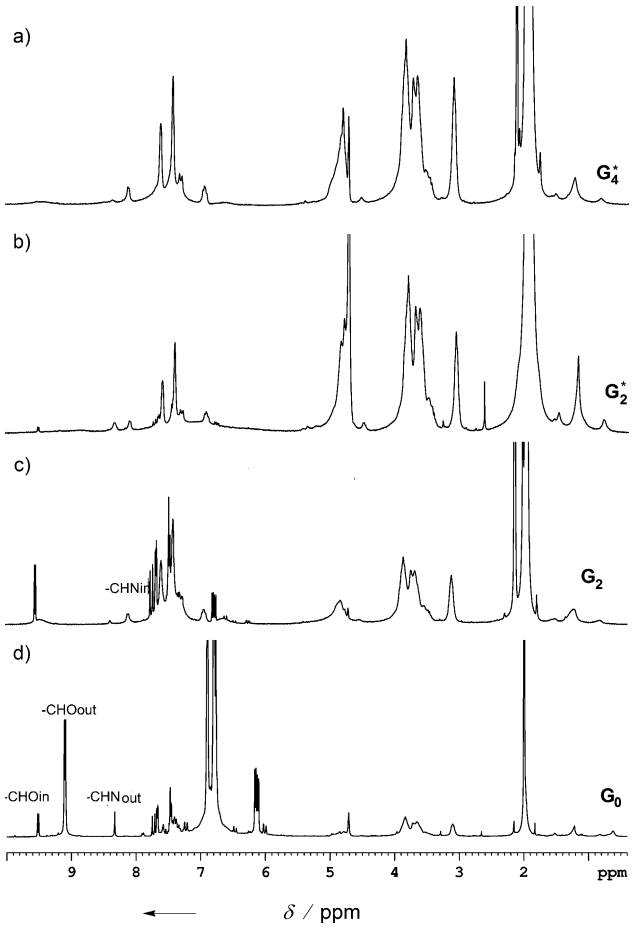

Figure 1. HR-MAS spectra of the $\mathbf{G_0}$, $\mathbf{G_2}$, $\mathbf{G_2}$*, and $\mathbf{G_4}$ hydrogels ($-CHO_{in}$, $-CHO_{out}$, $-CHN_{in}$, and $-CHN_{out}$ are the "in-water" and "out-of-water" aldehyde and imine protons, respectively; see Scheme 1 and Table 1 for further details and the composition of hydrogels, respectively).

Table 2. Chitosan conversion into cinnamimine–chitosan.

Yield	$\mathbf{G_0}$*	$\mathbf{G_1}$	$\mathbf{G_1}$*	$\mathbf{G_2}$	$\mathbf{G_2}$*	$\mathbf{G_3}$	$\mathbf{G_3}$*	$\mathbf{G_4}$	$\mathbf{G_4}$*
η_{in} [a]	28.7	32.9	21	29	20.5	16.1	10.3	13.4	11.7
η_{out} [b]	38.3	16.2	29.7	7.5	20.7	9.8	20.1	9.5	12.5
η_{total} [c]	67	49.1	50.7	36.5	41.2	25.9	30.4	22.9	24.2
η_{solid} [d]	nd	90.1	nd	46.8	nd	29.7	nd	23.7	nd
η_{max} [e]	100	100	100	50	50	33.3	33.3	25	25

[a] η_{in} is the yield of imine formation in water. [b] η_{out} is the yield of imine formation out of water. [c] η_{total} is the total yield of imine formation calculated from the HR-MAS spectra by using the equation $\eta = (A_{CH=N})/(A_{H2} \times 0.865) \times 100$, where $A_{CH=N}$ and A_{H2} are the areas of the imine and amine adjacent the H2 protons of **C**, respectively (0.865 reflects the degree of deacetylation). [d] η_{solid} is the yield of imine formation in the solid state calculated from ^{13}C NMR solid-state spectra. [e] η_{max} is the maximum possible yield according to molar ratio of the reagents. nd = not determined.

Interestingly enough, the HRMAS spectra of the **G** hydrogels kept for one week at room temperature (**G***) show that the aldehyde groups are progressively converted into imino groups, mostly present in "out-of-water" configurations (Figure 1). The total yield η_{total} and "in-water" η_{in} or "out-of-water" η_{out} yields of the imine formation were determined to have better quantitative insight into the gelation process (Table 2).

As for the imine-bond formation in **G*** hydrogels, the "in-water" yields decrease while the "out-of-water" yields increase relative to fresh hydrogels **G**. The progressive imine-bond formation induces an increase of the concentration of the imino-bound **Cy** groups, which further induces a specific self-organization process through the segregation of "out-of-water" hydrophobic **Cy**/"in-water" hydrophilic **C** layers (Scheme 1). The solution/solid phase-transformation processes, including the removal of water, are highly beneficial for increasing the yield η_{solid} of imine-bond formation (Table 2).[3]

Despite the low solubility of **Cy**, it is important to note that "out-of-water" imino-bond formation is very close to the η_{max} value in the solid state (Table 2), thus suggesting strong

constitutional correlation of reversible molecular imino-bond formation and supramolecular self-assembly of hydrophobic (**Cy**)/hydrophilic (**C**) mesophases during the dynagel formation.

ATR-FTIR spectroscopic analysis

Additional evidence of imine-bond formation was provided by attenuated total reflectance (ATR)-FTIR spectroscopic analysis. The IR spectra of chitosan and **C**/**Cy** xerogels are presented in Figures 2 and 3. **Cy** presents strong five overlapped bands in the region of $\tilde{\nu}=3700–2700\ cm^{-1}$ (i.e., $\tilde{\nu}=3356$, 3286, 3208, 3102, and $3034\ cm^{-1}$; evidenced from the second derivative spectrum), with a maximum at $\tilde{\nu}=3328\ cm^{-1}$. These bands are assigned to different OH stretching vibrations: the secondary OH group at the C3 position forms a hydrogen bond with the O5 atom of the adjacent ring (C3-H3···O5 intramolecular hydrogen bond), the primary OH group at the C6 position is involved in a hydrogen bond with the O3 atom in the neighboring chain (C6-H6···O3′ intermolecular hydrogen bond), and also the NH intra- and intermolecular hydrogen bonds.

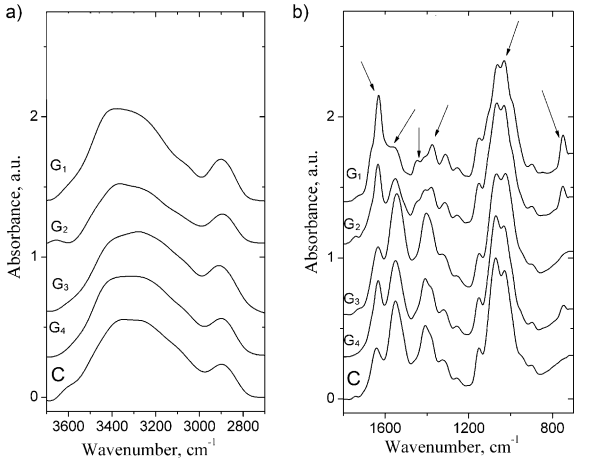

Figure 2. FTIR spectra of chitosan (**C**) and chitosan–cinnamaldehyde $\mathbf{G_1}$–$\mathbf{G_4}$ hydrogels in the regions a) $\tilde{\nu}=3700–2700$ and b) 1800–700 cm^{-1}.

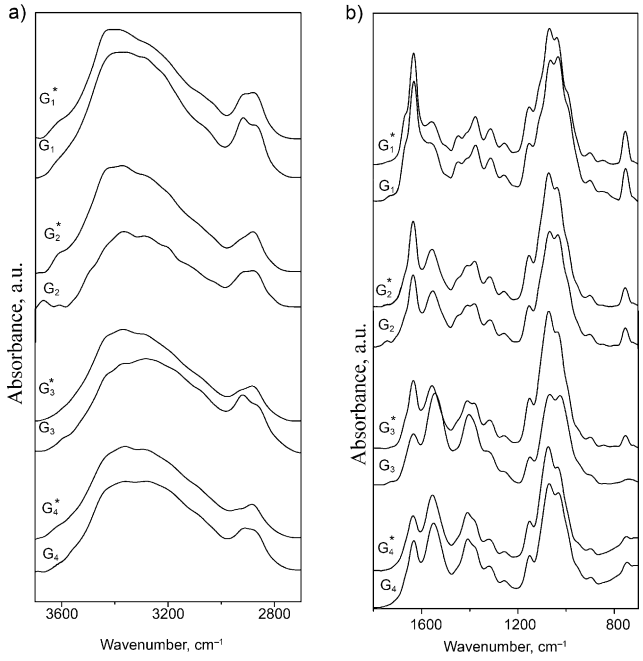

Figure 3. FTIR spectra of **G** and **G*** chitosan–cinnamaldehyde hydrogels in the regions a) $\tilde{\nu}=3600–2700$ and b) 1800–700 cm^{-1}.

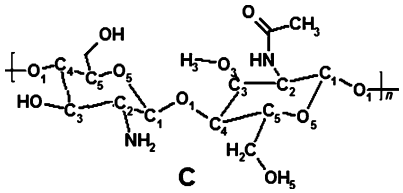

The bands assigned to symmetric and antisymmetric $-CH_2$ stretching vibrations are located at $\tilde{\nu}=2914$, 2882, and $2859\ cm^{-1}$.

Significant bands were evidenced in the fingerprint region at $\tilde{\nu}=1638$, 1551 and $1256\ cm^{-1}$, which were assigned to the -C=O (amide I), NH (amide II), and HNCO (amide III) stretching vibrations, respectively. The bands that correspond to symmetric and antisymmetric deformation vibrations of CH_2, CH_3, and CH groups appeared at $\tilde{\nu}=1409$, 1380, and $1325\ cm^{-1}$, respectively. The spectral band located at $\tilde{\nu}=1151\ cm^{-1}$ was assigned to the symmetric structure of the C-O-C groups, whereas the broad bands at $\tilde{\nu}=1031$ and $1063\ cm^{-1}$ indicated the C–O stretching vibration in primary and second OH groups, and the band located at $\tilde{\nu}=897\ cm^{-1}$ is due to the pyranose-ring vibrations.

The IR spectra of the xerogels **G** and **G*** show clear modifications relative to the chitosan spectrum due to the imine-bond formation (Figure 3).

One can observe an increase in intensity of the band located at $\tilde{\nu}=3102\ cm^{-1}$ and a small shift to a higher wavenumber of bands located at $\tilde{\nu}=3357$ and $3224\ cm^{-1}$, thus suggesting the disappearance of the NH groups involved in hydrogen-bond formation and a redistribution of the hydrogen bonds. With an increase of the degree of substitution, a sharp band at $\tilde{\nu}=1628\ cm^{-1}$, is evidenced in the fingerprint region. This band partially overlaps with the band located at $\tilde{\nu}=1638\ cm^{-1}$ and is assigned to group stretching vibrations of the newly formed C=N bond between chitosan and cinnamaldehyde. This assignment is confirmed by the decrease of and shift to higher wavenumbers of the band at $\tilde{\nu}=1551\ cm^{-1}$, which is assigned to the NH_2 groups. The IR spectra of the xerogels also indicate the presence of the stretching vibration of the C=C groups from the aromatic ring at $\tilde{\nu}=1446\ cm^{-1}$ and the presence of the CH bending vibration of the aromatic ring at $\tilde{\nu}=748\ cm^{-1}$. Relative to the chitosan IR spectrum, a variation in the intensity of bands for the C–O groups involved in primary and secondary hydrogen bonds can be seen in the xerogel spectra, thus suggesting a reorganization of the hydrogen bonds.

The IR spectra of the **G** and **G*** xerogels show the same characteristic bands. However, the **G*** spectra show clear modifications relative to the **G** spectra in terms of shifting of the bands to higher or lower wavenumbers and intensity variation. Therefore, a new band appears at $\tilde{\nu}=3430\ cm^{-1}$, which is as-

signed to the formation of new intermolecular hydrogen bonds, in the spectra of **G*** xerogels.[27] The band located at $\tilde{\nu}=3359\ cm^{-1}$ in the **G** xerogels spectra is shifted to a higher wavenumber of $\tilde{\nu}=3370\ cm^{-1}$, thus suggesting weaker intramolecular hydrogen bonds. The band at $\tilde{\nu}=2864\ cm^{-1}$, which is assigned to the stretching vibration of CH_2 groups, is shifted to a higher wavenumber of $\tilde{\nu}=2877\ cm^{-1}$ and presents an intensity increase, which is attributed to an increase in the degree of ordering.[28] At the same time, the band located at $\tilde{\nu}=1563\ cm^{-1}$ in the FTIR spectra of **G**, which is assigned to the stretching vibration of NH_2 groups, is shifted to a lower wavenumber in the FTIR spectra of **G***. Generally, the region of $\tilde{\nu}=1500–1200\ cm^{-1}$ gives information about the local symmetry – the variation in intensity, band frequency, and/or shape are strongly affected by the inter- or intramolecular hydrogen bonding of OH groups. The bands at $\tilde{\nu}=1415$ and $1375\ cm^{-1}$ are assigned to CH_2 bending due to the rearrangements of hydrogen bonds on the most favorable orientation of the primary OH groups and CH bending and the C–CH_3 deformation mode, respectively. For **G*** xerogels, these bands show a shape modification and slight shifting to a higher wavenumber, thus suggesting a modification in the environment of CH_2OH groups, although the high degree of bond coupling in this region makes it difficult to assess the type of chain packing or hydrogen-bonding network. On the other hand, the bands at $\tilde{\nu}=1063$ and $1030\ cm^{-1}$, assigned to the C–O stretching vibration in the C6–OH and C3–OH groups, are shifted to a higher wavenumber and, at the same time, the intensity of the band at $\tilde{\nu}=1063\ cm^{-1}$ increases. All the above described modifications in the FTIR spectra of **G*** relative **G** point to mostly intermolecular rearrangements due to different interactions between the **C**/**Cy** components. As a main conclusion, the importance of the intermolecular hydrogen bonds increases while that of the intramolecular hydrogen bonds decreases. A rational explanation for this conclusion is that the chitosan chains are coiled in the **G** xerogels, thus facilitating the intramolecular linkages, whereas the chitosan chains are straighter in the **G*** xerogels due to the self-assembled rigid cinnamaldehyde–imine domains, thus hindering the intramolecular forces and facilitating the intermolecular forces.

SEM

SEM micrographs reveal that the xerogels obtained by lyophylization of the G_1–G_4 and G_1*–G_4* hydrogels present a porous spongelike microstructure (Figure 4). The diameter of the pores and their polydispersity progressively increases for the G_1–G_4 xerogels from 8 to 50 μm with a decreasing **Cy** content (i.e., the thickness of the walls is about 150 nm). In a close correlation, mass equilibrium swelling (MES) was observed to be higher for the samples with a lower **Cy** content that present a higher porosity (see the Supporting Information for a detailed discussion about the swelling behavior of xerogels). The confinement of a high amount of water in the hydrogels with a high **C** content during xerogel-pore formation increases the pore size. However, the G_1–G_4 xerogels are morphologically quite inhomogeneous relative to the more compact G_1*–G_4*

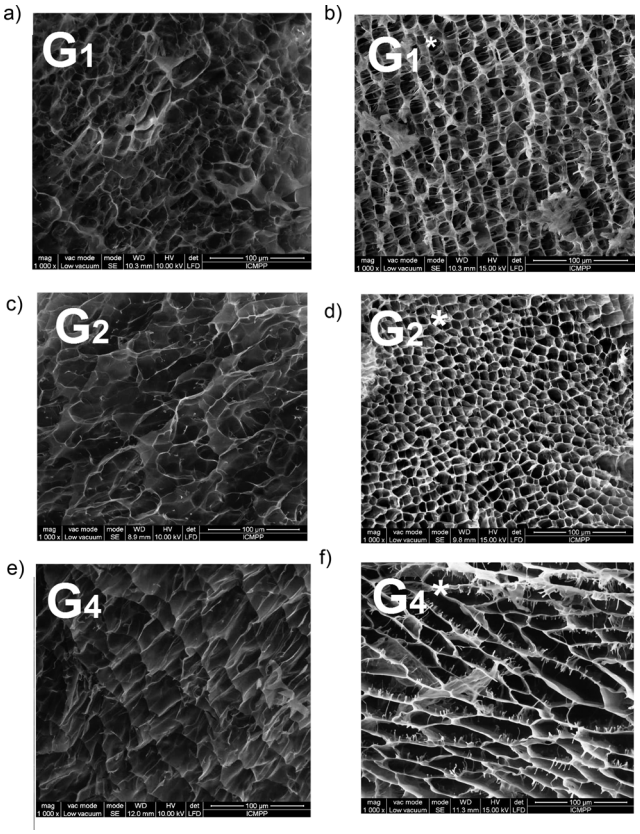

Figure 4. SEM micrographs of the lyophilized hydrogels a) G_1, b) G_1*, c) G_2, d) G_2*, e) G_4, and f) G_4*.

xerogels (i.e., 10 and 40 μm for G_1*–G_3* and G_4*, respectively), for which the pore-diameter polydispersity decreases. It is interesting to note a long-range organization of the G_1*–G_4* xerogels toward a higher arrangement of the pores. This phenomenon certainly depends on the superior emergence of outer-hydrophilic/inner-hydrophobic domains in the walls of the pores, thus regulating the innerpore amount of water during pore formation much better. Interestingly enough, the xerogel with the lowest **Cy** content G_4* presents innerpore "pins" on the walls, probably formed by the free-chitosan chain segments solvated within innerpore water during pore formation.

XRD

Further valuable insight into the self-organization of chitosan hydrogels was obtained from XRD analysis of the pellet xerogel samples of the G_1–G_4 xerogels (obtained by lyophilization of fresh hydrogels) and the G_1*–G_4* xerogels (obtained by lyophilization of the hydrogels kept for one week; Figure 5). In this regard, the evolution of the wide-angle XRD pattern was also recorded of a fresh hydrogel over 5 days.

The XRD patterns of pure chitosan films show broad peaks of low intensity at $2\theta\cong12^\circ$ and $2\theta\cong21^\circ$, which correspond to d-spacings of 7.4 and 4.3 Å, respectively, thus indicating the presence of the crystalline form II of hydrogen-bonded, highly deacetylated chitosan[3b,29] (Figure 5). Relative to **C**, the XRD

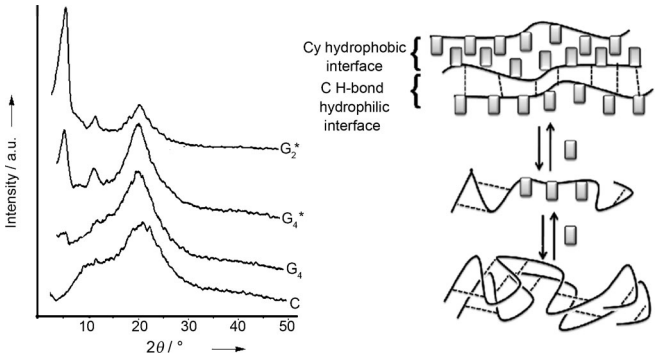

Figure 5. XRD patterns of **C** and the G_4, G_4*, and G_2* hydrogels. Possible structural self-organization of polymeric **C** backbones (black lines) are progressively grafted with **Cy** (gray rectangles).

patterns of the G_1–G_4 xerogels do not show remarkable differences, except for a weak broad band in the small-angle region ($2\theta \cong 5^\circ$, d-spacing of 17.6 Å), which corresponds to the length of the interdigitated cinnamaldehyde layer. The XRD patterns of the **G1**–**G4** xerogels strongly evidence the nonperiodic **Cy** incorporation into the chitosan backbones, which increases the interchain distances and disturbs the hydrogen-bonding network of **C** in an irregular manner (Figure 5).

On the other hand, the XRD patterns of the G_1*–G_4* xerogels are indicative of the self-organized lamellar nanophases, thus exhibiting three sharper bands at $2\theta \cong 5$, 11, and 20°, respectively, which correspond to d-spacings of 18.0 (i.e., the length of the double interdigitated cinnamaldehyde layer),[30] 8.0 (i.e., **C** hydrogen-bonding interchain distance), and 4.5 Å (i.e., π–π stacking distance between the phenyl moieties), respectively, and are reminiscent of ordered mesomorphic polyazomethines.[31,32] The important gain of reflection intensity is correlated with increasing concentration of **Cy** (G_4*→G_1*) and consequently with a longer range order due to the progressive "out-of-water" incorporation of **Cy** in the chitosan backbones. It can be seen that the interchain distances are a little bit longer relative to the chitosan distances (7.4 Å), thus indicating disruption of the intramolecular hydrogen bonds and the preponderant presence of intermolecular hydrogen bonds, as confirmed by the FTIR spectra.

To understand the mechanistic details of constitutional hydrogel formation through molecular imino-bond dynamics and supramolecular self-organization better, the XRD diffraction measurements were performed repeatedly on fresh hydrogels at pre-established time intervals. Although the fresh hydrogels show only an amorphous broad peak at $2\theta \cong 27$ °, thus indicating the presence of hydrogen bonding with water molecules,[33] the X-ray diffractograms drastically change with time and are in agreement with **G*** formation within 24 hours, thus remaining practically unchanged for more than 100 hours when the dry hydrogel state is reached. Interestingly enough, the XRD pattern recorded of the ground dried hydrogel shows a similar pattern, but with an important loss of low-angle reflection intensity, thus indicating lower crystallinity.[34]

Swelling behaviors

The swelling behavior of **C**/**Cy** xerogels was analyzed in water, buffer solution at pH 7.4, and dried alcohol and compared to chitosan. The swelling increases first rapidly and then slowly to reach a maximum constant swelling (see Table 3 for the MES)

Table 3. Mass equilibrium swelling (MES) of the studied hydrogels.

Solvent	Chitosan	G1	G2	G4	G1*	G_2*	G_4*
alcohol	2.6	16.8	24.6	26.6	21.0	22.3	24.4
water	–[a]	17.9	26.4	37.3	22.7	25.5	41.4
buffer (pH 7.4)	–[a]	2.6	5.4	5.9	8.3	3.5	5.3

[a] Not measured due to the dissolution of the sample.

within about 48 hours in alcohol and within approximately 5 days in water and the buffer solution at pH 7.4. The amount of absorbed water at pH 7 in the hydrogel network was almost similar to that in alcohol and drastically larger than that at pH 7.4 measured at the same time intervals. The MES is directly related to **Cy** content and xerogel morphology. Thus, the MES value is higher for the samples with a lower **Cy** content and, consequently, higher porosity. The swelling curves in alcohol and the buffer solution are given as an example in Figure 3.

Relative to chitosan, the greater porosity of the **C**/**Cy** xerogels, the MES of which is about ten orders of magnitude higher, is obvious. Although chitosan xerogels disintegrate in water and the buffer solution, the **C**/**Cy** xerogels reach the MES in a few days, thus indicating that the studied xerogels become more hydrophobic due to the **Cy** units. Remarkably, the G_4/G_4* swelling progress in water causes loosening of the gel and reaches a high erosion rate after 5 days, in a similar manner to chitosan xerogels, but slower, most probably due to a lower **Cy** content.

Rheological measurements

A gel-like behavior is indicated by rheological measurements for all the samples except G_5 – the minimum amount of cinnamaldehyde to obtain chitosan gelation is a 22.2:1 molar ratio to the number of amine groups. High viscosity and elastic behavior are observed with an increased content of **Cy**, which is reminiscent of the formation of the compact and elastic networks (total recovery *R* is approximately 80 %) due to mechanically adaptive self-assembled **Cy**.[35]

The frequency sweep measurements determined in the linear viscoelastic regime indicated a gel-like behavior ($G' > G''$) for all the samples, except G_5 which showed a liquidlike behavior ($G' < G''$). Accordingly, the minimum amount of cinnamaldehyde to obtain chitosan gelation was established as a 4.5:1 molar ratio of the amino to chitosan and aldehyde groups (Figure 4S a). The increasing frequency does not significantly affect the values of G' and G''; that is, the gel is not broken down by the mechanical shear force. The G'-storage modulus is higher than G''-loss modulus, which illustrates that strong interactions

between the chitosan backbones are developed by the **Cy** cross-linker. On the other hand, the *G*′-storage modulus, ascribed to the strain-energy reversibility stored in the sample, increases along with an increase in the amount of cinnamaldehyde cross-linker, thus indicating an increasing number, strength of the interactions in the system and, therefore, an increasing linking density (Figure 4S b).[36]

The complex viscosity η^* decreases with increasing the oscillation frequency for the **G** hydrogel samples, thus indicating a shear-thinning behavior (i.e., pseudoplastic material). This viscosity decrease, along with an increase in the velocity gradient, can be attributed to a structural change of the hydrogel network; that is, the chitosan backbones align according to flow direction leading to a viscosity decrease. Higher viscosity is observed for a higher **Cy** concentration, thus suggesting a more compact network in which **Cy** has a reinforcing effect (Figure 4S c). Thus, although the complex viscosity of the hydrogel sample studied with a low **Cy** percentage ($\mathbf{G_5}$) decreases insignificantly in the investigated frequency range, an increase in the **Cy** amount ($\mathbf{G_{4.5}}$–$\mathbf{G_2}$) determines an increase in the η^* value of two orders of magnitude at a given oscillation frequency.

For the hydrogel samples containing lower **Cy** amounts ($\mathbf{G_{3.5}}$–$\mathbf{G_5}$), the temperature sweep tests show a slight increase of the *G*′ value starting at 20 °C, whereas the hydrogel samples containing higher **Cy** amounts ($\mathbf{G_2}$, $\mathbf{G_3}$) are stable, their storage modulus remaining constant over the whole investigated temperature range (Figure 4S d). The weak in increment the *G*′ value can be attributed to the temperature effect on the chitosan gels in terms of stretching and deprotonation effects.[37]

The creep and recovery tests, which inform about structural properties, were carried out at a shear stress in the linear viscoelastic region in which the applied stress is very small. A typical creep and recovery curve shows the variation of compliance *J* with time and is related to the softness of the sample; consequently, a higher *J* value indicates a weaker material structure and a lower *J* value defines a stronger material structure.[35] In the case of **C**/**Cy** hydrogels, the *J*-creep compliance value decreases as the amount of **Cy** in the sample increases, thus indicating a stronger elastic network structure, whereas the compliance–time dependence of the **G5** sample is typical for a system with liquid-like behavior characterized by a continuous deformation that begins at zero and a very small elastic recovery value (Figure 5). On the other hand, the percentage of total recovery *R*[38] revealed high values of around 80%, thus indicating a high elasticity degree conferred by the three-dimensional network of the hydrogel structure.

Conclusion

Cinnamimino–chitosan biodynamers have been obtained by condensation of cinnamaldehyde and chitosan. The present results reveal that imine-bond formation takes place "in water" and generates low-ordered hydrogels in the first stage of the process. The progressive formation of imino bonds further induces an "out-of-water" increased reactivity within interdigitated hydrophobic self-assembled layers of **Cy**, which has a protecting environmental effect against hydrolysis and leads to stabilization of the imine bonds (Scheme 1). The hydrophobic swelling due to the cinnamimino **Cy** layers at the interfaces reaches a critical step when lamellar self-organized hybrids are generated (24 h). This process induces an important adaptive restructuration on the micrometric scale and results in the formation of highly ordered microporous morphologies of high potential interest. It is important to note the morphological and structural properties of the resulted gels are strongly related to the amount of **C** and **Cy** components, thus determining adaptive hydrophilic/hydrophobic phase-segregation behaviors based on internal interactional mechanisms.

The combined features of synergetic dynamic reversible generation (i.e., imine-bond formation) and increased conversion by self-organization (i.e., hydrophobic/hydrophilic supramolecular segregation) recommend processes and species such as those presented herein for the development of a constitutional "self-fabrication" approach toward systems of increasing behavioral complexity. These features open up wide perspectives to imagining a fundamental transition from molecular/supramolecular design toward constitutional self-selection approaches, thus shortening the essential steps from molecular to nanometric/micrometric functional systems of potential addressability,[2] which can directly benefit the fields of chemical separations,[38] sensors,[39] or storage–delivery devices.[40]

Acknowledgements

This work was financially supported by the Romanian National Authority for Scientific Research, CNCS - UEFISCDI grant (project number PN-II-ID-PCCE-2011-2-0028) and the European Union's Seventh Framework Program (FP7/2007-2013) under grant agreement no. 264115 - STREAM.

Keywords: biodynamers · chitosan · constitutional dynamic chemistry · imines · gels · self-assembly

[1] a) J.-M. Lehn, *Chem. Soc. Rev.* **2007**, *36*, 151 – 160; b) *Constitutional Dynamic Chemistry, Top. Curr. Chem.* (Ed.: M. Barboiu) **2012**, Springer, Berlin; c) M. Barboiu, J.-M. Lehn, *Proc. Natl. Acad. Sci. USA* **2002**, *99*, 5201 – 5206; d) F. Dumitru, Y. M. Legrand, A. van der Lee, M. Barboiu, *Chem. Commun.* **2009**, 2667 – 2669.

[2] a) J.-M. Lehn, *Angew. Chem.* **2013**, *125*, 2906 – 2921; *Angew. Chem. Int. Ed.* **2013**, *52*, 2836 – 2850; b) M. Barboiu, *Chem. Commun.* **2010**, *46*, 7466 – 7476; c) E. Moulin, G. Cormos, N. Giuseppone, *Chem. Soc. Rev.* **2012**, *41*, 1031 – 1049; d) N. Giuseppone, *Acc. Chem. Res.* **2012**, *45*, 2178 – 2188; e) M. Barboiu, M. Ruben, G. Blasen, N. Kyritsakas, E. Chacko, M. Dutta, O. Radekovich, K. Lenton, D. J. R. Brook, J.-M. Lehn, *Eur. J. Inorg. Chem.* **2006**, 784 – 789; f) E. Busseron, Y. Ruff, E. Moulin, N. Giuseppone, *Nanoscale* **2013**, *5*, 7098 – 7140.

[3] a) L. Marin, B. C. Simionescu, M. Barboiu, *Chem. Commun.* **2012**, *48*, 8778 – 8780; b) L. Marin, I. Stoica, M. Mares, V. Dinu, B. C. Simionescu, M. Barboiu, *J. Mater. Chem. B* **2013**, *1*, 3353 – 3358.

[4] a) C. Arnal-Hérault, A. Pasc-Banu, M. Barboiu, M. Michau, A. van der Lee, *Angew. Chem.* **2007**, *119*, 4346 – 4350; *Angew. Chem. Int. Ed.* **2007**, *46*, 4268 – 4272; b) C. Arnal-Hérault, M. Barboiu, A. Pasc, M. Michau, P. Perriat, A. van der Lee, *Chem. Eur. J.* **2007**, *13*, 6792 – 6800; c) M. Michau, M. Barboiu, R. Caraballo, C. Arnal-Hérault, P. Periat, A. van der Lee, A. Pasc, *Chem. Eur. J.* **2008**, *14*, 1776 – 1783; d) G. Gottarelli, G. P. Spada, *Chem.*

Rec. **2004**, *4*, 39 – 49; e) A. Ghoussoub, J. M. Lehn, *Chem. Commun.* **2005**, 5763 – 5765; f) N. Sreenivasachary, J.-M. Lehn, *Proc. Natl. Acad. Sci. USA* **2005**, *102*, 5938 – 5943; g) R. Nguyen, E. Buhler, N. Giuseppone, *Macromolecules* **2009**, *42*, 5913 – 5915; h) L. Tauk, A. P. Schröder, G. Decher, N. Giuseppone, *Nat. Chem.* **2009**, *1*, 649 – 654.

[5] J. Vinsova, E. Vavrikova, *Curr. Pharm. Des.* **2008**, *14*, 1311 – 1326.

[6] R. Jayakumar, M. Prabaharan, S. V. Nair, S. Tokura, H. Tamura, N. Selvamurugan, *Prog. Mater. Sci.* **2010**, *55*, 675 – 709.

[7] R. A. A. Muzzarelli, *Carbohydr. Polym.* **2011**, *84*, 54 – 63.

[8] a) A. Montembault, C. Viton, A. Domard, *Biomacromolecules* **2005**, *6*, 653 – 662; b) X. Liu, J. S. Dordick, *J. Am. Chem. Soc.* **1999**, *121*, 466 – 467.

[9] E. B. Mirzaei, A. S. A. Ramazani, M. Shafiee, M. Danaei, *Int. J. Polym. Mater.* **2013**, *62*, 605 – 611.

[10] S. Kumar, J. Koh, *Int. J. Biol. Macromol.* **2012**, *51*, 1167 – 1172.

[11] S. Lin-Gibson, H. J. Walls, S. B. Kennedy, E. R. Welsh, *Carbohydr. Polym.* **2003**, *54*, 193 – 199.

[12] A. Singh, S. S. Narvi, P. K. Dutta, N. D. Pandey, *Bull. Mater. Sci.* **2006**, *29*, 233 – 238.

[13] F. W. Kari, National Toxicology Program, *Toxicity Report Series* **1993**, No 25.

[14] H. Katagiri, T. Yamamoto, A. Uchimura, M. Tsunoda, Y. Aizawa, H. Yamauchi, *Ind. Health* **2011**, *49*, 328 – 337.

[15] P. Subash Babu, S. Prabuseenivasan, S. Ignacimuthu, *Phytomedicine* **2007**, *14*, 15 – 22.

[16] Y.-L. Xue, H.-X. Shi, F. Murad, K. Bian, *Vascular Health Risk Manag.* **2011**, *7*, 273 – 280.

[17] G. Brackman, T. Defoirdt, C. Miyamoto, P. Bossier, S. Van Calenbergh, H. Nelis, T. Coenye, *BMC Microbiol.* **2008**, *8*, 149.

[18] A. O. Gill, R. A. Holley, *Appl. Environ. Microbiol.* **2004**, *70*, 5750 – 5755.

[19] N. Sanla-Ead, A. Jangchud, V. Chonhenchob, P. Suppakul, *Packag. Technol. Sci.* **2012**, *25*, 70 – 117.

[20] S. S. Cheng, J.-Y. Liu, E.-H. Chang, S.-T. Chang, *Bioresour. Technol.* **2008**, *99*, 5145 – 5149.

[21] C. W. Lee, D. H. Hong, S. B. Han, S. H. Park, H. K. Kim, B. M. K. Won, H. M. Kim, *Planta Med.* **1999**, *65*, 263 – 266.

[22] S. J. T. Gowder, D. Halagowder, *J. Med. Sci.* **2012**, *2*, 101 – 109.

[23] J. Wang, Z. Lian, H. Wang, X. Jin, Y. Liu, *Appl. Polym. Sci.* **2012**, *123*, 3242 – 3247.

[24] V. Nipun Babu, S. Kannan, *Int. J. Biol. Macromol.* **2012**, *51*, 1103 – 1108.

[25] L. Chen, Z. Chen, X. Li, W. Huang, X. Li, X. Liu, *Polymer* **2013**, *54*, 1739 – 1745.

[26] R. Novoa-Carballal, E. Fernandez-Megia, R. Riguera, *Biomacromolecules* **2010**, *11*, 2079 – 2086.

[27] Y. Sun, L. Lin, H. Deng, J. Li, B. He, R. Sun, P. Ouyang, *BioResources* **2008**, *3*, 297 – 315.

[28] K. V. Harish Prashanth, F. S. Kittur, R. N. Tharanathan, *Carbohydr. Polym.* **2002**, *22*, 27 – 33.

[29] Y. Zhang, C. Xue, Y. Xue, R. Gaoa, X. Zhang, *Carbohydr. Res.* **2005**, *340*, 1914 – 1917.

[30] M. T. Kirchner, D. Bla, R. Boese, T. S. Thakur, G. R. Desiraju, *Acta. Cryst. C* **2011**, *67*, o387 – o390.

[31] H. Kim, W. Zin, *Polym. Bull.* **1997**, *39*, 701 – 705.

[32] L. Marin, E. Perju, M. D. Damaceanu, *Eur. Polym. J.* **2011**, *47*, 1284 – 1299.

[33] M. Xin, M. Li, K. Yao, *Macromol. Symp.* **2003**, *200*, 191 – 197.

[34] P. H. Hermans, A. Weidinger, *J. Am. Chem. Soc.* **1946**, *68*, 2547 – 2552.

[35] N. Sozer, *Food Hydrocolloids* **2009**, *23*, 849 – 855.

[36] D. S. Morais, M. A. Rodrigues, T. I. Silva, M. A. Lopes, M. Santos, J. D. Santos, C. M. Botelho, *Carbohydr. Polym.* **2013**, *95*, 134 – 142.

[37] S. P. Rwei, T. Y. Chen, Y. Y. Cheng, *J. Biosci. J. Biomater. Sci. Polymer Ed.* **2005**, *16*, 1433 – 1445.

[38] a) G. Nasr, T. Macron, A. Gilles, E. Petit, M. Barboiu, *Chem. Commun.* **2012**, *48*, 7398 – 7400; b) Y. Le Duc, M. Michau, A. Gilles, V. Gence, Y.-M. Legrand, A. van der Lee, S. Tingry, M. Barboiu, *Angew. Chem.* **2011**, *123*, 11568 – 11574; *Angew. Chem. Int. Ed.* **2011**, *50*, 11366 – 11372; c) A. Cazacu, Y.-M. Legrand, A. Pasc, G. Nasr, A. van der Lee, E. Mahon, M. Barboiu, *Proc. Natl. Acad. Sci. USA* **2009**, *106*, 8117 – 8122; d) M. Barboiu, C. Guizard, N. Hovnanian, J. Palmeri, C. Reibel, C. Luca, L. Cot, *J. Membr. Sci.* **2000**, *172*, 91 – 103; e) M. Barboiu, C. Guizard, C. Luca, N. Hovnanian, J. Palmeri, L. Cot, *J. Membr. Sci.* **2000**, *174*, 277 – 286.

[39] a) E. Mahon, T. Aastrup, M. Barboiu, *Chem. Commun.* **2010**, *46*, 5491 – 5493; b) E. Mahon, T. Aastrup, M. Barboiu, *Chem. Commun.* **2010**, *46*, 2441 – 2443; c) G. B. Rusu, F. Cunin, M. Barboiu, *Angew. Chem.* **2013**, *125*, 12829 – 12833; *Angew. Chem. Int. Ed.* **2013**, *52*, 12597 – 12601.

[40] a) A. Herrmann, *Angew. Chem.* **2007**, *119*, 5938 – 5967; *Angew. Chem. Int. Ed.* **2007**, *46*, 5836 – 5863; b) A. Herrmann, G. Godin, B. Levrand, A. Trachsel, J.-M. Lehn, *Chem. Commun.* **2010**, *46*, 3125 – 3127; c) Y. Le Duc, A. Gilles, S. Mihai, V. Rouessac, S. Tingry, M. Barboiu, *Chem. Commun.* **2013**, *49*, 3667 – 3669.

Received: December 2, 2013
Revised: January 6, 2014
Published online on March 11, 2014